Revised: 28 February 2021 | Accepted: 24 March 2021

DOI: 10.1002/ese3.897

RESEARCH ARTICLE

Energy Science & Engineering
Open Access

Optimization of wavy fin-and-elliptical tube heat exchanger using CFD, multi-objective genetic algorithm and radical basis function

Chao Yu[1] | **Xiangyao Xue**[1] | **Kui Shi**[1] | **Renhao Wang**[2] | **Lei Zhang**[1] | **Mingzhen Shao**[1]

[1]Changchun Institute of Optics, Fine Mechanics and Physics, Chinese Academy of Sciences, Changchun, China

[2]Military Representative Office of Rocket Equipment Department in Harbin, Harbin, China

Correspondence
Chao Yu, Changchun Institute of Optics, Fine Mechanics and Physics, Chinese Academy of Sciences, Changchun 130033, China.
Email: yuchao@ciomp.ac.cn

Abstract

This article presents an accurate and efficient optimization method for heat exchanger. The structure of the original heat exchanger was optimized by combining LHS sampling, CFD simulation, radical basis function, and multi-objective optimization. Since the Colburn factor *j* and the friction factor *f* are a pair of conflicting goals, so the multi-objective optimization is adopted. The optimization results showed that the Colburn factor *j* increased by 5.43% and the friction factor *f* decreased by 23.31%, indicating that the optimized structure had higher heat transfer efficiency and lower resistance performance. The heat transfer mechanism and optimization effect of heat exchanger are explained by using the field synergy principle, which provides a theoretical basis for the structural design optimization of heat exchanger.

KEYWORDS

CFD, field synergy, multi-objective optimization, tube heat exchanger

1 | INTRODUCTION

The fin-and-elliptical tube heat exchanger is a kind of compact heat exchanger with fins and tubes. It is widely used in vehicles, engineering machinery, refrigeration, aerospace, and other fields. Depending on the various application, the fins have different styles such as slit fin,[1,2] perforated fin,[3,4] louvered fin,[5,6] and wavy fin.[7,8] The tube shape is circular or elliptical. In recent years, with the development of numerical simulation and experiment, wavy fin-and-elliptical tube heat exchangers have been paid more and more attention.

A large number of scholars have carried out detailed numerical analysis of the wavy fin-and-elliptical tube heat exchangers. Bhuiyan et al[9] grouped and summarized the influence of different types of heat exchangers. They found that the heat transfer performance of wavy fin was better than that of plain fin. Matos et al[10] found that the optimal elliptic tube has higher heat exchange, compared with the circular tube. Tao et al[11] discovered that for elliptic arrangements, the heat transfer of fin and tube heat exchanger are enhanced, when the Reynolds number and fin thickness increased. Lotfi et al[12] showed that the thermal and hydraulic performance can be enhanced by improving the Reynolds number, increasing the height of the corrugated fin and decreasing the ovality of the tube. Damavandi et al[13] used the group method of data handling type neural network to multi-objective optimize for maximum heat transfer and minimum pressure drop. Chen et al[14] determined the fin temperature and heat transfer coefficient for the smaller tube. The temperature and velocity distributions of air between the two fins have also confirmed.

The scholars also conducted experimental studies on the thermodynamic properties of fin-and-tube heat exchangers.

Wang et al[15] experimentally studied the effects of the number of tube rows, fin pitch, and edge corrugation on the air-side performance. They found that the heat transfer characteristics were strongly related to the corrugation angle, and the ratio of waffle height and wave length. Marković et al[16] studied the air side pressure drop in plate finned tube heat exchangers. Based on the experimental data, they established a reliable procedure for estimation of air pressure drop by newly introduced parameters such as velocity and others.

In order to obtain better fluid mixing and heat transfer efficiency at low Reynolds number, Gongnan Xie[17] optimized the geometric shape of electronic radiator corrugated channels with the application of construction theory to minimize the overall thermal resistance and improve the thermal performance of structural corrugated channels. Based on the constructal theory, Yidan Song[18] studied dimensionless variables such as channel space, wavelength ratio, and amplitude ratio, and obtained the optimal configuration of the wave fin-channels for the compact heat exchanger applied in the heat recovery system of micro-turbine.

The performance of the laser fin-and-elliptical tube heat exchanger (WFET heat exchanger) was determined by the structure size of its fin and tube. Hence, the four main dimensions of the elliptical radiator were selected as variables to obtain Colburn factor j and friction factor f in this paper. A large Colburn factor j and a small friction factor f were targeted for optimization. The optimal structure size was obtained through radical basis function (RBF) and genetic algorithm (MOGA). Finally, comparison with the original model verifies the rationality of optimization.

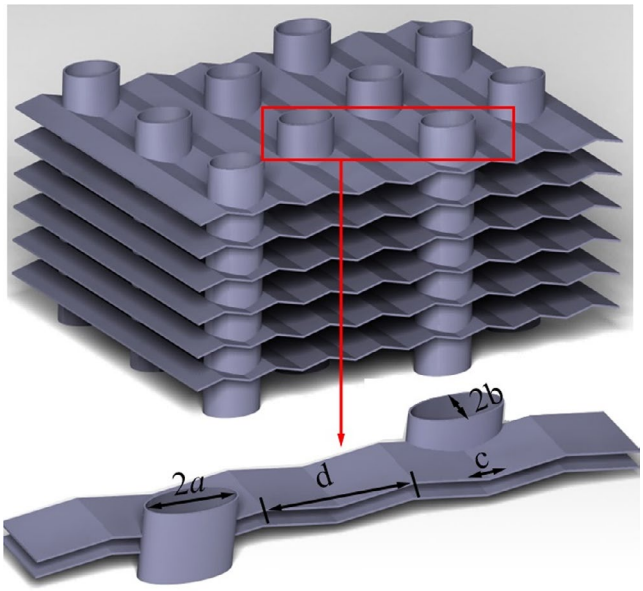

FIGURE 1 WFET heat exchanger model

2 | STRUCTURE PARAMETERS OF WFET HEAT EXCHANGERS

In the field of engineering, the heat dissipation efficiency of WFET heat exchanger determines the service life and reliability of machine. In order to obtain the proper structure parameters of the heat exchanger, a kind of WFET heat exchanger is studied. Its' 3D model and structure parameter is shown in Figure 1 and Table 1. When the heat exchanger works, the cold fluid (low temperature coolant air) and hot fluid (high temperature liquid) flow through the tube and fin made of aluminum, respectively.

3 | NUMERICAL SIMULATION OF WFET HEAT EXCHANGERS

3.1 | Boundary conditions

The inner structure of the heat exchanger is intricate, and the flow is also a complex process. The distribution characteristics of the flow field in the flow channel through CFD are obtained by solving fluid dynamics equation and heat transfer equation. The three conservation laws are widely used to solve various mass and heat transfer problems, and the differential form of conservation laws used in this article is shown in Equations (1)-(3).[19]

Continuity equation:

$$\frac{\partial \rho}{\partial t} + \nabla \cdot \left(\rho \cdot \vec{u}\right) = 0 \tag{1}$$

Momentum conservation equation:

$$\frac{d\vec{u}}{dt} = \vec{F} - \frac{\Delta P}{\rho} = 0 \tag{2}$$

Energy conservation equation:

$$\rho \frac{dH}{dt} = \frac{dp}{dt} + \nabla \cdot (k \nabla T) + \varphi \tag{3}$$

TABLE 1 Values of structural parameters

Fin dimensions	Values	Tube dimensions	Values
Fin corrugated angle (°)	150.66	Major axes of tube (mm)	6.875
Fin spacing (mm)	13.75	Minor axis of tube (mm)	6.875
Fin thickness (mm)	0.5	Tube thickness (mm)	0.5

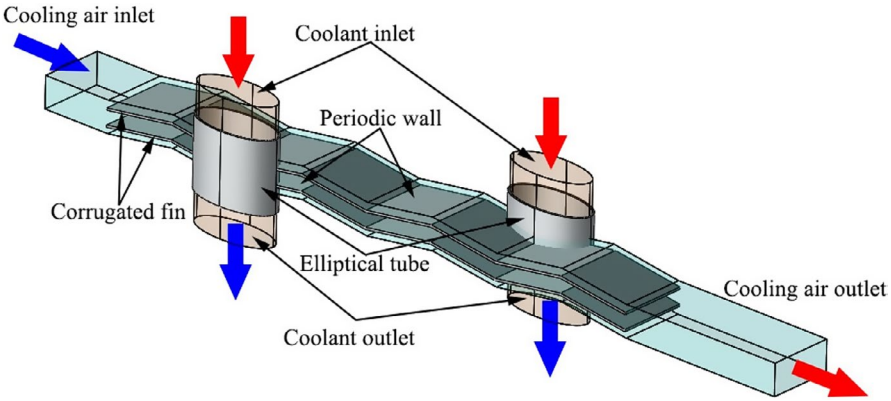

FIGURE 2 Boundary conditions instruction

TABLE 2 Related physical properties

	Water	Air	Aluminum
Density [kg/m^3]	998.2	1.23	2719
Specific heat [J/(kg K)]	4182	1006.43	871
Thermal conductivity [W/(m K)]	0.6	0.0242	237
Viscosity [Pa s]	8.81×10^{-4}	2.493×10^{-5}	-

where u is the flow velocity vector, t is the time, H is the enthalpy, k is the thermal conductivity of the fluid, and φ is the viscous dissipation function.

The characteristics of single channel correspond to the overall performance of the heat exchanger. The single channel model was extracted to save the computation time, as shown in Figure 2. The inlet face of single channel is velocity inlet. The cold inlet fluid is 8 m/s and the temperature 27°C, while the hot inlet fluid is 2 m/s and the temperature 77°C.[9-12] The two outlet faces are set as pressure outlet. The cooling air surrounding walls are set as periodic walls. The number of cycles is set to 15, as the actual radiator size. The coupled equations of pressure and velocity are solved by RNG k-ε model.

3.2 | Numerical setting

The ANSYS Fluent software is selected as the CFD solver to work out the governing equations by using the finite volume method.[13,14] The convection term in governing equation is solved by SIMPLE algorithm and second-order upwind scheme. The physical properties of fluid and solid can be found in Table 2.

The computational domain of single channel model is discretized with hexahedral mesh by Ansys mesh as shown in Figure 3. The mesh size of the first layer near the wall is 0.1 mm ($y+ < 5$), the growth rate of the encrypted mesh is 1.2, and the mesh size of the mainstream area is 0.25 mm. In order to improve the accuracy of simulation, seven grid results with different number of mesh are compared with proved grid independence. The number of meshes was 258 731, 285 549, 309 867, 342 312, 363 618, 377 483, 423 772, and 451 261, respectively. The Nusselt number what represents the ratio of thermal conductivity resistance to convective heat transfer resistance of the fluid layer is an important parameter to characterize heat transfer effect. Therefore, the optimal mesh number is calculated by combining Nusselt number and time cost. With the increasing of meshes, the computation time increases gradually and the Nusselt number flattens out, as shown in Figure 4. Considering the simulation accuracy and time cost, the grid number is set as 377 483, in this research.

3.3 | Comparison with the experiment

A series of different Reynolds numbers are calculated by CFD to compare with the experimental results,[20] as shown in Figure 5. The simulation results are basically consistent with the experimental results. The root-mean-square error of Nu is about 9.7%. Within the margin of error, it can be considered that the numerical model has accuracy and reliability.

4 | THE EFFECT OF STRUCTURAL PARAMETER

The relationship between the structure and performance of the heat exchanger is described by j and f.

4.1 | Major axis of tube a

The Figure 6A shows the effect of major axis of tube a on the j and f, when the other structural size are $b = 7$ mm, $c = 150°$, $d = 12.5$ mm. With the increase of a, the Colburn factor j and

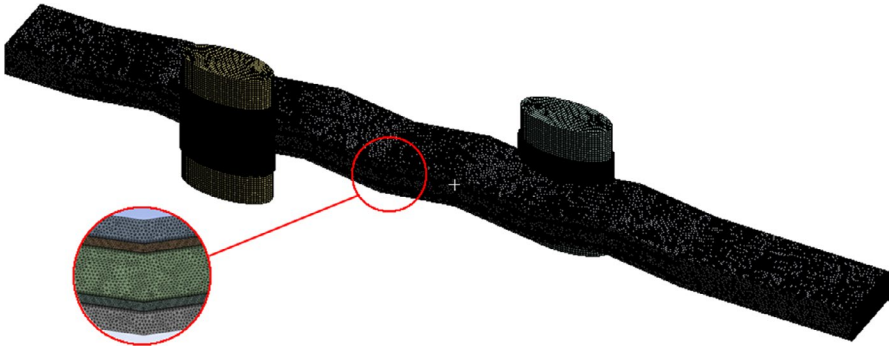

FIGURE 3 The gird for computational domain

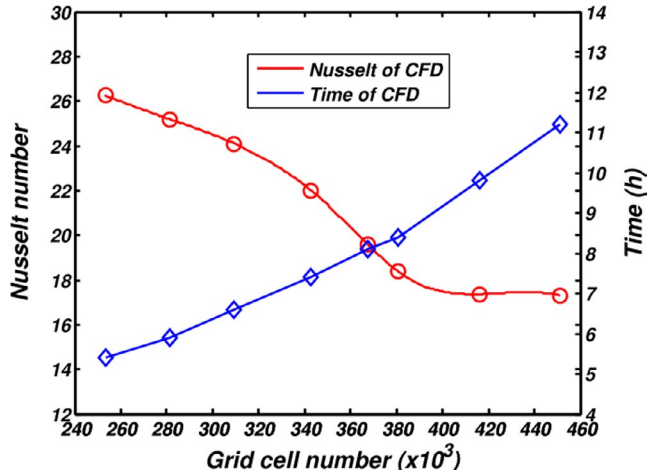

FIGURE 4 Grid independence verification

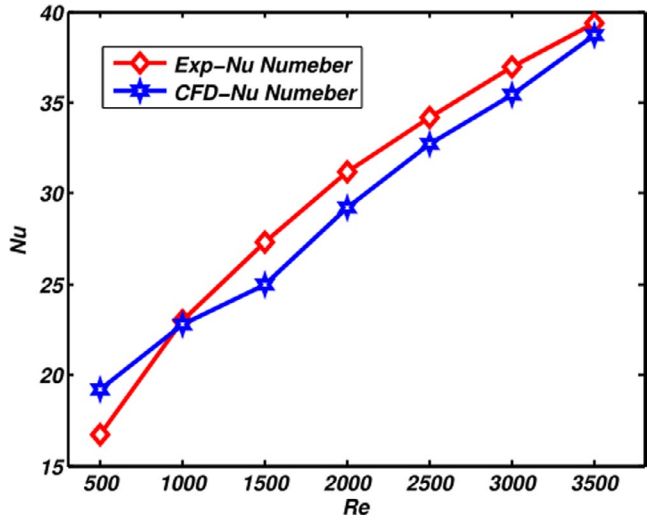

FIGURE 5 Comparison of experimental and simulated *Nu* values

friction factor *f* both increase to 20% and 30%, respectively. Meanwhile, the ascending gradient of friction factor *f* is gradually higher than that of Colburn factor *j*. The Colburn factor *j* of a larger *a* is not the maximum value, but the friction factor *f* is relatively low and has a higher *j*/*f* value. With a certain value of *b*, a larger *a* increases the area of primary heat transfer between air and pipe and occupies a larger flow passage space at the same time. In short, a slightly larger *a* can improve the heat exchange performance of the heat exchanger.

4.2 | Minor axis of tube *b*

The Figure 6B shows the effect of minor axis of tube *b* on the *j* and *f*, when the other structural size $a = 7.5$ mm, $c = 150°$, $d = 12.5$ mm. As shown in Figure 11B, both Colburn factor *j* and friction factor *f* increase with the increase of minor axis of tube *b*. When the minor axis of tube *b* is large, the fin flow passage section becomes smaller, and the resistance to fluid flow increases significantly. As the minor axis of tube b is large, it forms a phenomenon similar to jet flow when the fluid flows to the wall of the elliptical tube, which also improves the heat transfer efficiency of the fluid. In general, a larger *b* significant affects fluid flow, and excessively high resistance puts forward higher performance requirements for inlet wind speed. So a smaller minor axis of tube *b* is more appropriate.

4.3 | Fin corrugated angle *c*

The Figure 6C shows the influence of fin-corrugated angle *c* on the *j* and *f*, when other structural parameters are $a = 7.5$ mm, $b = 7$ mm, and $d = 12.5$ mm. With the fin-corrugated angle *c* gradually increases, both the Colburn factor *j* and friction factor *f* gradually decrease. When the fin-corrugated angle *c* approaches 150°, the change of *f* decreases. The wavy fins gradually approach to straight fins and the flow resistance decreases with the increase of fin-corrugated angle *c*. At the same time, the turbulence generated by the fluid passing through the fins is reduced, and the convective heat transfer efficiency is reduced. Therefore, the fin-corrugated angle *c* with a small change in *f* is selected to have a lower value of *f* and a higher value of *j*.

4.4 | Fin spacing *d*

The Figure 6D shows the influence of fin-corrugated angle *c* on the *j* and *f*, when other structural parameters are

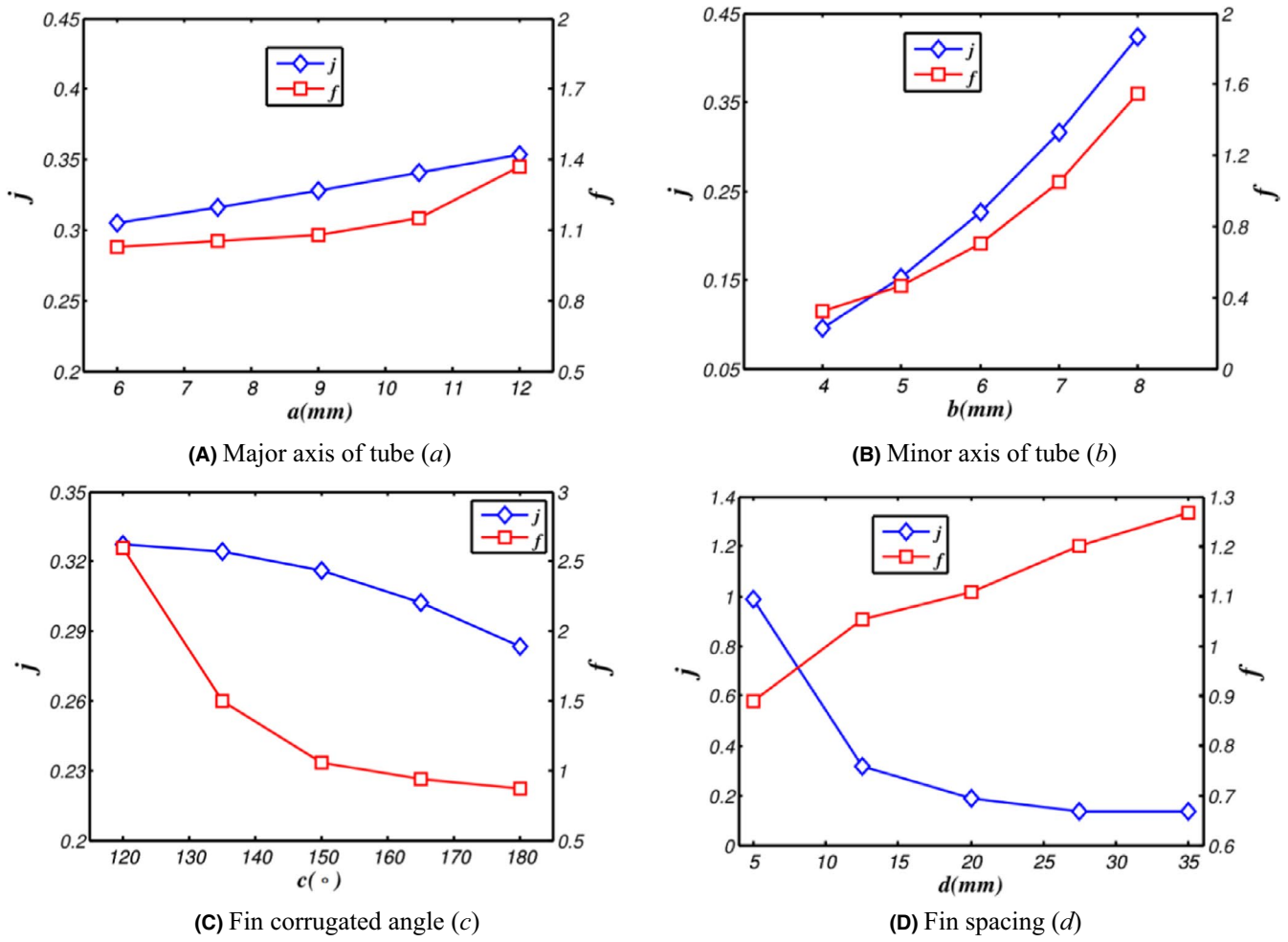

(A) Major axis of tube (a)

(B) Minor axis of tube (b)

(C) Fin corrugated angle (c)

(D) Fin spacing (d)

FIGURE 6 Influence of design parameters on heat transfer performance

a = 7.5 mm, b = 7 mm, and c = 150°. The j gradually decreases and the friction factor f gradually increases with fin spacing d increases. When the fin spacing d is large, the fin bending is more obvious, and the air is subjected to greater resistance. Moreover, the vortexes are formed at the bend of the wavy fin to reduce the secondary heat transfer area. At the same time, the smaller the fin spacing is, the easier the heat exchanger is to compact. Therefore, a smaller fin spacing has a higher j/f, and the heat exchanger performance is better.

5 | OPTIMAL STRUCTURE OF WFET HEAT EXCHANGERS

In reality, many engineering problems have multiple goals. And these goals often contradict each other. The heat exchanger shape optimization is designed to achieve high heat transfer capability and low flow resistance. The high heat transfer capability represents a relatively complex structure. The low flow resistance indicates that the fluid in the channel is smooth, and the structure is relatively simple. So the heat transfer performance and flow resistance are a pair of contradictory goals. The RBF and multi-objective-based algorithm (MOGA) are used to obtain the optimal WFET heat exchanger structure parameters by considering the heat transfer performance and resistance performance.

The program flow diagram is shown in Figure 7. Firstly, the multi-objective optimization problem is defined and the range of influence factors is determined. Secondly, the design of experiment was carried out by Latin Hypercube sampling (LHS) to get the sample point data. Thirdly, the target factors of each sample are solved by CFD, and the approximate model is obtained by radical basis function (RBF). Finally, the optimal structure parameters of WFET heat exchanger is got by MOGA.

Step 1: Constraint condition

The high heat transfer efficiency and low flow resistance are considered as excellent finned structures. The relevant data are being read from fluent simulation results. The larger Colburn factor j indicates higher heat transfer effect and the smaller friction factor f indicates lower flow resistance. The

objective of optimization is to make the structural parameters of the heat exchanger have a larger Colburn factor *j* factor and smaller *f* factor that can be expressed as follows:

$$\begin{cases} j = \dfrac{Nu}{R_e P_r^{1/3}} \\ f = \dfrac{2\Delta P D}{\rho u^2 L} \end{cases} \tag{4}$$

Nu, *Re*, and *Pr* are *Nusselt* number, *Reynolds* number, and *Prandtl* number. They are defined as:

$$\begin{cases} D = \dfrac{4S}{U} = \dfrac{4s(h-t)}{2[s+(h-t)]} = \dfrac{2s(h-t)}{s+h-2t} \\ Re = \dfrac{\rho D u}{\mu} \\ Pr = \dfrac{\mu c_p}{\lambda} \\ Nu = \dfrac{m c_p D (T_{out} - T_{in})}{\lambda S \Delta t_m} \end{cases} \tag{5}$$

The impact factor are major axes of tube *a*, minor axes of tube *b*, fin corrugated angle *c*, fin spacing *d*. The objective function is shown as follows:

$$F(X) = F(x_1, x_2, x_3, x_4) = F(a, b, c, d) \tag{6}$$

The WFET heat exchanger structural parameters are[15,16,21]:

$$6 < a < 12, 4 < b < 8, 120 < c < 180, 5 < d < 35. \tag{7}$$

The largest *j* and the smallest *f* are defined as the function (8).

$$\begin{aligned} maxj(x_i) &= maxF(a, b, c, d) \\ minf(x_i) &= minF(a, b, c, d) \end{aligned} \tag{8}$$

Step 2: Design of experiments (DOE)

Because of the nonlinear relationship between structure parameters and performance, 50 sample points are selected by Latin Hypercube Sampling (LHS) to study the interaction effect (parameters listed in Appendix A). LHS, a stratified random sampling, is capable of efficiently sampling from the distribution interval of variables, assuming that there are now n variables $x_1, x_2, \ldots, x_n$. To take K samples from their specified interval, the cumulative distribution of each variable is divided into the same K cells. A value is randomly selected from each interval, and K values of each variable are randomly combined with the values of other variables. Different from random sampling, this method can ensure the full coverage of each variable range by maximizing the stratification of each edge distribution. The 3D models are constructed and simulated.

Step 3: Approximation model

The RBF algorithm is applied to obtain the approximation model which can be expressed as[22]:

$$y = \sum_{i=1}^{n} w_{ij} \exp\left(-\frac{n}{2\sigma^2} \left\| x_p - c_i \right\|^2 \right) \tag{9}$$

where w_{ij} is the weight of the neurons between the hidden layer and the output layer, σ is the variance of basis function, n is the number of sample, and c_i is the center of clustering.

The approximate relationship between the influence factor and the optimization objective is determined by RBF. Another 20 sets of sample points are select to prove the accuracy of approximate model. The low RMSE can be considered that the approximate model is rational and usable. Its equation is shown in Equation (10).

$$\mathrm{RMSE} = \sqrt{\left[\sum\nolimits_{i=1}^{n} (X_{\mathrm{CFD}} - X_{\mathrm{model}})^2 \right] / n} \tag{10}$$

The nonlinear relationship between the influence factor and performance can be obtained by the results solved by CFD, shown in Appendix C.

Step 4: Multi-objective optimization

The optimal structure of the approximate model is obtained by multi-objective optimization.

6 | OPTIMAL RESULT ANALYSIS

The structure parameters *a*, *b*, *c*, and *d* with the maximum *j*/*f* are obtained through the above steps, as shown in Table 3.

TABLE 3 Structural parameters before and after optimization

	a (mm)	*b* (mm)	*c* (°)	*d* (mm)
Before optimization	6.875	6.875	150.66	13.75
After optimization	8.108	4.214	139.32	10.28

TABLE 4 CFD and approximate model comparison

	j	*f*
CFD	0.31	0.49
Approximation	0.22	0.53
Error	4.09%	7.54%

FIGURE 7 Optimization process

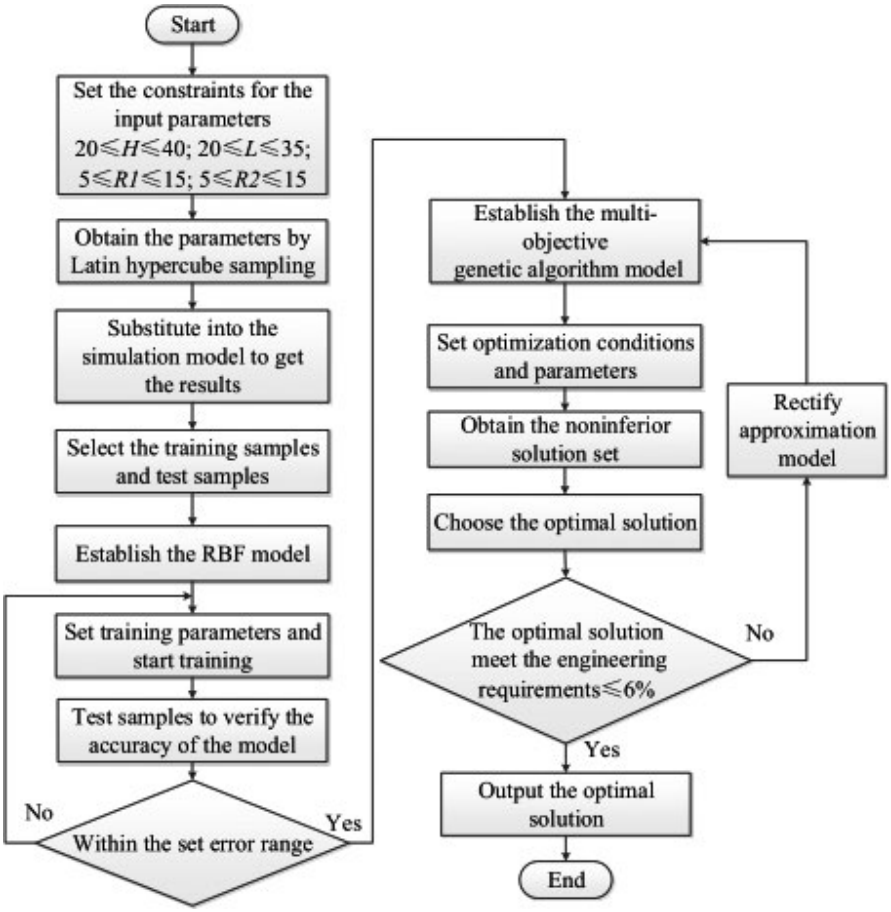

FIGURE 8 The optimization and original models (The gray model is the original, the purple model is the optimization)

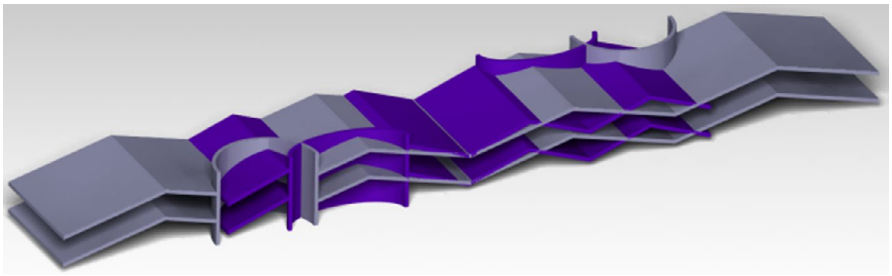

Table 4 shows the j and f obtained by the approximate model and CFD with the optimized model. The comparison error between the two results is less than 10%, and the accuracy of the approximate model is verified. The Figure 8 shows the difference between the original structure and the optimized structure.

The Figure 9 compares the velocity, temperature, and pressure of the optimized model with the original model at the section $z = 0$. As the fluid flows through the fin, the pressure gradually decreases and the temperature gradually increases. Although the temperature difference between the inlet and outlet of the optimized finned structure is slightly larger than 4.6 K; the pressure difference between inlet and outlet of the optimized fin structure is 21.8 Pa, which is 10% less than the original structure. At the same inlet velocity, the cold air flow efficiency is higher, which is more in line with the needs of heat transfer in engineering.

In the original model, the turbulent kinetic energy of the fluid near the wall was low, because the fluid in the boundary layer was greatly affected by the wall viscosity force. That belongs to laminar flow with high thermal resistance. In the optimized model, the impact effect of fluid on fins is obvious. This effectively destroys the laminar flow near the wall, reduces the boundary layer thickness, and further improves the heat transfer efficiency.

In general, a good performance evaluation criterion is the basis of optimal design of heat exchanger structure. Here, the ratio of the thermal performance coefficient η which considers pressure losses and Nusselt number is designated as an evaluation criterion for the structure optimization. The η is defined as the function (11).

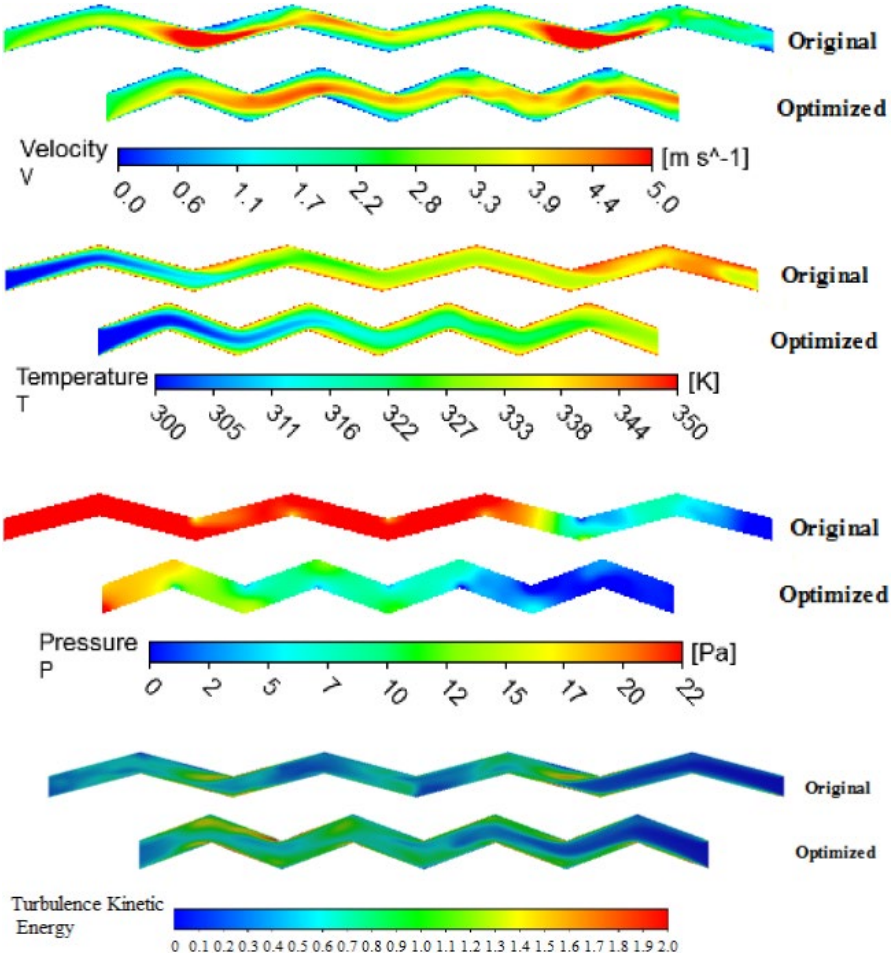

FIGURE 9 Comparison transverse section between the optimization and the original

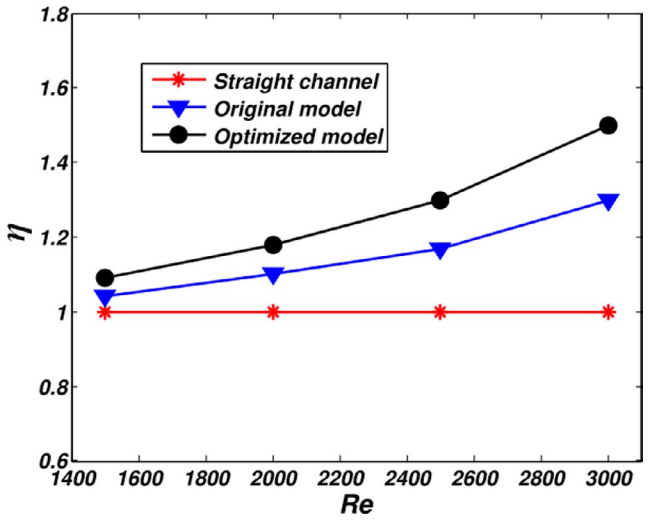

FIGURE 10 The η compared between the original and optimized model

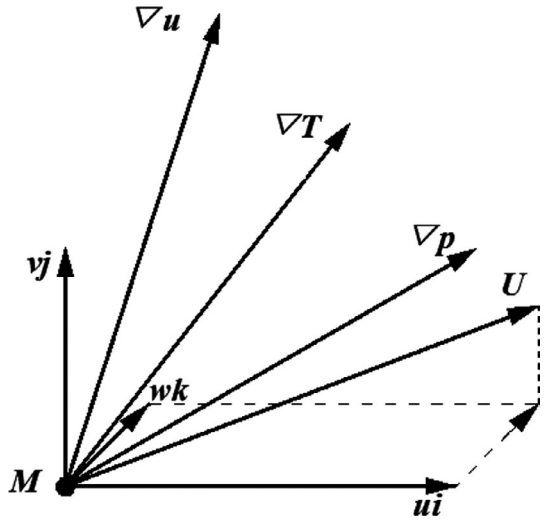

FIGURE 11 The vector and gradient of particle M in the flow field[25]

$$\eta = [Nu/Nus] / [f/fs] \tag{11}$$

The Nu and Nus are defined as the Nu of wavy and straight channel, respectively. The f and fs are defined as the f of wavy and straight channel, respectively. The η of the original and optimized model is compared, as shown in the Figure 10.

To sum up, although the temperature difference is slightly increased after optimization, the frictional resistance of the fin structure is reduced, the heat exchange capacity is enhanced.

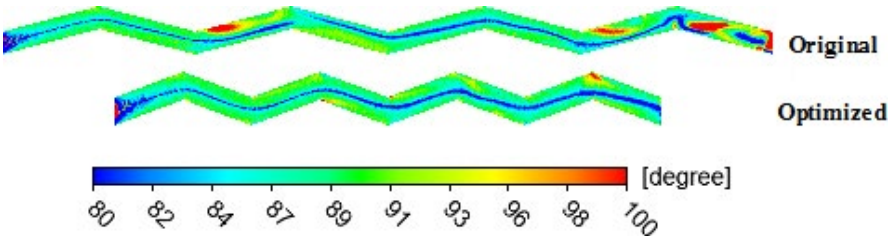

FIGURE 12 Comparison of synergy angle β

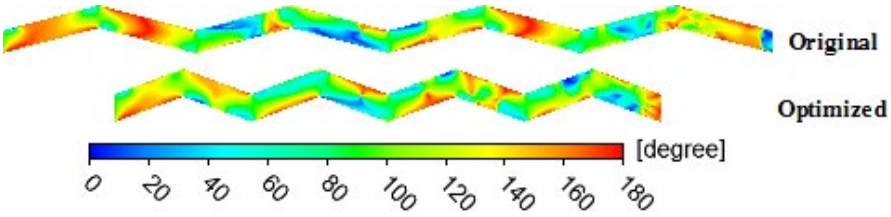

FIGURE 13 Comparison of synergy angle θ

The thermal performance coefficient η of optimized model is higher than the original model.

7 | RESULTS AND DISCUSSION

The optimization of wavy fin-and-elliptical tube heat exchanger involves two key problems. First, the influence of the change of single size structure on the performance of heat exchanger provides designers with design guidance. Second, how to better understand the mechanism of heat transfer and the results of enhanced heat transfer corresponding to structural changes.

The transfer mechanism of convective heat transfer in heat exchanger can be analyzed by the field synergy theory.[23] Under the same boundary conditions of velocity and temperature, the synergy degree of velocity field and temperature field in the flow passage is better, and the heat transfer performance is better. In this research, the field synergy principle is introduced to evaluate the heat exchanger. Figure 11 shows the relationship between the physical fields. The quantity of field synergy is shown as follows[24]:

$$\begin{cases} \beta = arccos \frac{U \cdot \nabla T}{|U||\nabla T|} \\ \theta = arccos \frac{U \cdot \nabla p}{|U||\nabla p|} \\ \gamma = arccos \frac{\nabla T \cdot \nabla u}{|\nabla T||\nabla u|} \end{cases} \tag{12}$$

The angle between the velocity vector and the temperature gradient is the synergy angle β, which represents the heat transfer efficiency between fins and fluids. The synergy angle θ between the velocity vector and the pressure gradient represents the resistance of fluid to flow through the channel. The synergy angle γ represents the angle between the temperature gradient and the velocity gradient, which represents the contrast between heat transfer and flow resistance.

7.1 | Field synergy angle β

The Figure 12 shows the synergy angle β of original and optimized model in the same position of the flow channel ($z = 0$). When the cold fluid flows through the fin, the hot fluid transfers heat through the fin, and the temperature gradient is perpendicular to the fluid velocity vector. According to the field synergy theory, the synergy angle β is approaching 90° near the wall. There is smaller synergy angle β of optimized model, which represent the higher heat transfer efficiency.

7.2 | Field synergy angle θ

The Figure 13 shows the synergy angle θ of original and optimized model in the same position of the flow channel ($z = 0$). The synergy angle distributions of the two models are similar. The airflow obstruction at the fin bend leads to the deviation between the near wall flow and the main flow direction. Therefore, the larger θ suggests higher resistance. Generally, the angle θ of the optimized model is obviously smaller.

7.3 | Field synergy angle γ

The Figure 14 shows the synergy angle γ of original and optimized model in the same position of the flow channel ($z = 0$). We all know that the larger synergy angle γ is, the stronger the heat transfer capacity will be. It is also found in the figure that the synergy angle γ near the fin bend are larger, indicating that there is the main heat transfer area.

To sum up, the synergy angle β and synergy angle θ of the optimization model are relatively small as shown in Table 5.

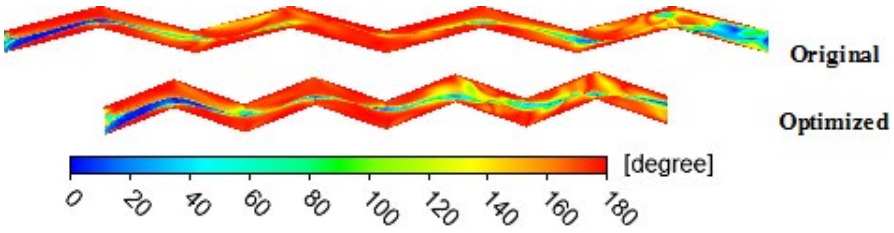

FIGURE 14 Comparison of synergy angle γ

TABLE 5 The mean synergy angle before and after optimization

	β	θ	γ
Before optimization	95.21	94.62	146.03
After optimization	90.16	91.06	151.32

This indicate that it has higher heat transfer effect and lower resistance effect. At the same time, the larger γ value is defined as better heat transfer performance. Above analysis process and method can explain the heat exchange principle of the WFET and also confirm the more reasonable optimized structure.

8 | CONCLUSION

In this paper, the wavy fin-and-elliptical tube heat exchanger was selected as the research object. The LHS was used for sampling, the flow field data were obtained through CFD, and the wavy fin and elliptical tube structures were optimized by RBF and MOGA. After optimization, the Colburn factor j of the structure increased by 5.43%, and the friction factor f decreased by 23.31%, showing a significant improvement effect. Then, the flow field inside the heat exchanger was analyzed to verify the optimization effect. The optimized air temperature increased by 4.6 K, the pressure drop decreased by 10%, and the speed also increased. Finally, the heat transfer mechanism and optimization effect are explained by using the field synergy principle, and the effect of optimization structure is further verified, which provides a theoretical basis for guiding the structural design optimization of heat exchanger.

ACKNOWLEDGMENTS

The work reported in this paper is supported by State Key Laboratory of Laser Interaction with Matter, Changchun Institute of Optics, Fine Mechanics and Physics, Chinese Academy of Sciences.

ORCID

Chao Yu https://orcid.org/0000-0002-1768-239X

REFERENCES

1. Wang C-C, Tao W-H, Chang C-J. An investigation of the air-side performance of the slit fin-and-tube heat exchangers. *Int J Refrig*. 1999;22(8):595-603. https://doi.org/10.1016/S0140-7007(99)00031-6
2. Li J, Wang S, Chen J, Lei Y-G. Numerical study on a slit fin-and-tube heat exchanger with longitudinal vortex generators. *Int J Heat Mass Transfer*. 2011;54(9-10):1743-1751.
3. Liu X, Yu J, Yan G. A numerical study on the air-side heat transfer of perforated finned-tube heat exchangers with large fin pitches. *Int J Heat Mass Transfer*. 2016;100:199-207.
4. Lee DH, Jung JM, Ha JH, Cho YI. Improvement of heat transfer with perforated circular holes in finned tubes of air-cooled heat exchanger. *Int Commun Heat Mass Transfer*. 2012;39(2):161-166.
5. Leu J-S, Liu M-S, Liaw J-S, Wang C-C. A numerical investigation of louvered fin-and-tube heat exchangers having circular and oval tube configurations. *Int J Heat Mass Transfer*. 2001;44(22):4235-4243.
6. Erbay LB, Uğurlubilek N, Altun Ö, Doğan B. Numerical investigation of the air-side thermal hydraulic performance of a louvered-fin and flat-tube heat exchanger at low Reynolds numbers. *Heat Transfer Eng*. 2017;38(6):627-640.
7. Wang CC, Fu WL, Chang CT. Heat transfer and friction characteristics of typical wavy fin-and-tube heat exchangers. *Exp Therm Fluid Sci*. 1997;14(2):174-186.
8. Glazar V, Trp A, Lenic K. Numerical study of heat transfer and analysis of optimal fin pitch in a wavy fin-and-tube heat exchanger. *Heat Transfer Eng*. 2012;33(2):88-96.
9. Bhuiyan AA, Islam AKMS. Thermal and hydraulic performance of finned-tube heat exchangers under different flow ranges: a review on modeling and experiment. *Int J Heat Mass Transf*. 2016;101:38-59.
10. Matos RS, Vargas JVC, Laursen TA, Bejan A. Optimally staggered finned circular and elliptic tubes in forced convection. *Int J Heat Mass Transf*. 2004;47(6-7):1347-1359.
11. Tao YB, He YL, Wu ZG, Tao WQ. Three-dimensional numerical study and field synergy principle analysis of wavy fin heat exchangers with elliptic tubes. *Int J Heat Fluid Flow*. 2007;28(6):1531-1544.
12. Lotfi B, Sundén B, Wang Q. An investigation of the thermo-hydraulic performance of the smooth wavy fin-and-elliptical tube heat exchangers utilizing new type vortex generators. *Appl Energy*. 2016;162:1282-1302.
13. Darvish Damavandi M, Forouzanmehr M, Safikhani H. Modeling and Pareto based multi-objective optimization of wavy fin-and-elliptical tube heat exchangers using CFD and NSGA-II algorithm. *Appl Therm Eng*. 2017;111:325-339.
14. Chen HT, Lin Y-S, Chen P-C, Chang J-R. Numerical and experimental study of natural convection heat transfer characteristics for

vertical plate fin and tube heat exchangers with various tube diameters. *Int J Heat Mass Transf*. 2016;100:320-331.
15. Wang CC. Investigation of wavy fin-and-tube heat exchangers: a contribution to databank. *Exp Heat Transfer*. 1999;12(1):73-89.
16. Marković S, Jaćimović B, Genić S, Mihailović M, Milovančević U, Otović M. Air side pressure drop in plate finned tube heat exchangers. *Int J Refrig*. 2019;99:24-29.
17. Xie G, Asadi M, Sunden B, Zheng S. Constructal theory based geometric optimization of wavy channels in the low Reynolds number regime. *J Electron Packag*. 2014;136(3):031013.
18. Song Y, Asadi M, Xie G, Rocha L. Constructal wavy-fin channels of a compact heat exchanger with heat transfer rate maximization and pressure losses minimization. *Appl Therm Eng*. 2015;75(6):24-32.
19. Yu C, Qin S, Liu Y, Chai B. Heat exchange performance optimization of a wheel loader cooling system based on computational fluid dynamic simulation. *Adv Mech Eng*. 2018;10(11):168781401880398.
20. Tao YB, He YL, Wu ZG, Tao WQ. Three-dimensional numerical study and field synergy principle analysis of wavy fin heat exchangers with elliptic tubes.
21. Kays WM, London AL. *Compact Heat Exchangers*; 1984.
22. Xie S, Xie Y, Huang T, Gui W, Yang C. Generalized predictive control for industrial process based on neuron adaptive splitting and merging RBF neural network. *IEEE Trans Industr Electron*. 2018;99:1.
23. Guo ZY, Tao WQ, Shah RK. The field synergy (coordination) principle and its applications in enhancing single phase convective heat transfer. *Int J Heat Mass Transf*. 2005;48(9):1797-1807.
24. Liu W, Liu ZC, Huang SY. Physical quantity synergy in the field of turbulent heat transfer and its analysis for heat transfer enhancement. *Sci Bull*. 2010;55(23):2589-2597.
25. Yu C, Xue X, Shi K, Shao M. A three-dimensional numerical and multi-objective optimal design of wavy plate-fins heat exchangers. *Processes*. 2021;9:9. https://doi.org/10.3390/pr9010009

How to cite this article: Yu C, Xue X, Shi K, Wang R, Zhang L, Shao M. Optimization of wavy fin-and-elliptical tube heat exchanger using CFD, multi-objective genetic algorithm and radical basis function. *Energy Sci Eng*. 2021;9:1359–1372. https://doi.org/10.1002/ese3.897

APPENDIX A

50 sets of structural parameters sample points

Code	*a* (mm)	*b* (mm)	*c* (°)	*d* (mm)	Code	*a* (mm)	*b* (mm)	*c* (°)	*d* (mm)
1	6.88	5.9	173.44	19.7	26	8.66	7.02	163.34	26.32
2	7.8	7.12	137.8	25.88	27	11.68	7.66	162.08	23.3
3	9.56	6.86	131.22	19.42	28	9.4	4.86	148.94	20.34
4	9.06	5.82	161.14	17.16	29	8.3	7.98	147.22	31.52
5	9.78	7.76	127.5	24.78	30	6.16	5.48	135.34	13.18
6	11.12	4.2	168.86	16.48	31	7.42	5	125.16	24.22
7	9.84	4.34	164.18	33.28	32	10.28	4.14	133.6	34.12
8	8.8	7.4	123.38	29.16	33	8.58	6.1	174.16	12.36
9	11.38	7.32	141.3	14.3	34	9.54	7.5	130.36	10.42
10	8.12	7.08	126.16	21.68	35	7.22	6.94	175.36	31.14
11	7.7	6.42	130.86	16.88	36	8.5	4.7	141.02	10.86
12	8.42	5.94	120.78	18.2	37	7.36	4.9	142.32	33.56
13	6.38	4.72	157.52	22.74	38	10.72	7.14	175.86	15.42
14	9.24	5.2	153.88	11.34	39	6.06	5.6	140.34	20.56
15	11.46	6.06	137.58	13.98	40	10.72	6.76	165.8	27.8
16	10.16	5.12	152.42	11.66	41	11.78	4.4	158.1	14.68
17	9.2	4.58	130.94	21.42	42	8	6.62	144.36	34.9
18	7.02	5.44	157.46	22.36	43	9	6.54	169.26	28.76
19	7.58	4.3	121.2	32.48	44	9.98	7.22	179.52	18.74
20	7.16	4.04	145.28	29.52	45	7.48	4.96	138.42	23.94
21	8.18	5.32	134.68	25.18	46	11.56	4.5	118.94	30.68
22	11.9	5.62	120.44	26.84	47	9.24	6.16	171.88	30.22
23	9.62	5.74	155.06	12.64	48	11.24	6.28	135.64	15.98
24	10.46	5.22	150.56	28.12	49	10.36	7.88	159.26	32.52
25	10.82	6.32	178	17.86	50	6.72	6.18	167.8	27.48

APPENDIX B

20 sets of contrast sample points

Code	*a* (mm)	*b* (mm)	*c* (°)	*d* (mm)	Code	*a* (mm)	*b* (mm)	*c* (°)	*d* (mm)
1	8.34	6.24	130.32	24.18	11	10.96	6.46	110.18	27.18
2	8.52	5.54	118.16	21.44	12	6.88	7.76	102.58	15.5
3	6.32	7.9	127.48	20.74	13	11.9	5.64	146.18	32.1
4	11.48	4.24	173.06	12.82	14	8.08	4.46	158.88	23.38
5	8.74	4.06	153.28	30.06	15	9.38	5.22	106.08	33.06
6	11.18	7.32	160.48	10.94	16	7.4	7.12	123.98	13.78
7	9.74	4.84	139.76	11.56	17	7.58	5.14	148.88	16.66
8	6.16	5.94	142.58	29.3	18	10.4	7.5	168.42	28.04
9	7.04	6.64	133.92	34.6	19	10.1	4.68	164.44	17.84
10	9.26	6.98	178.56	25.44	20	10.52	6.12	112.26	19

APPENDIX C

Non-linear relationship between parameters and performances

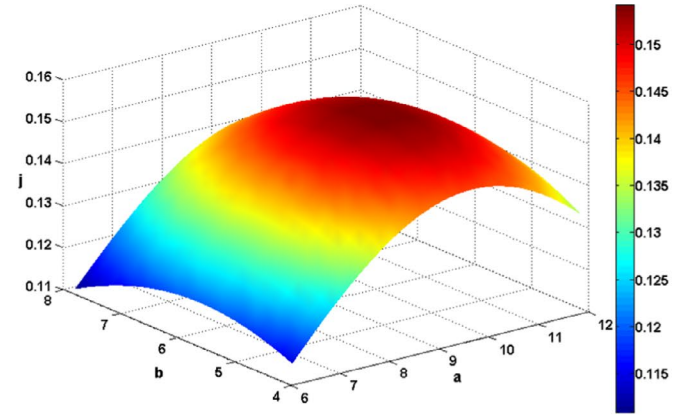

(A) *j vs b*, *a*

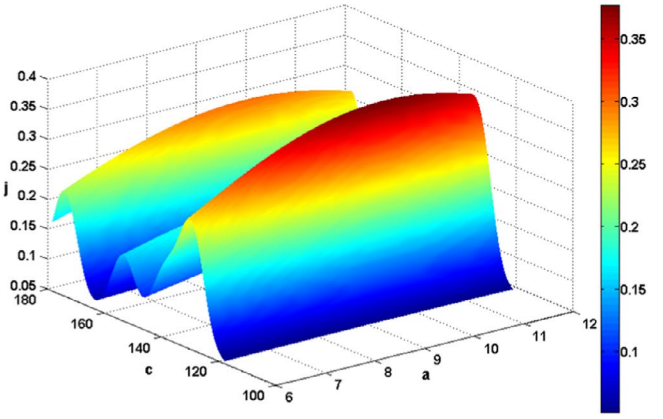

(B) *j vs c*, *a*

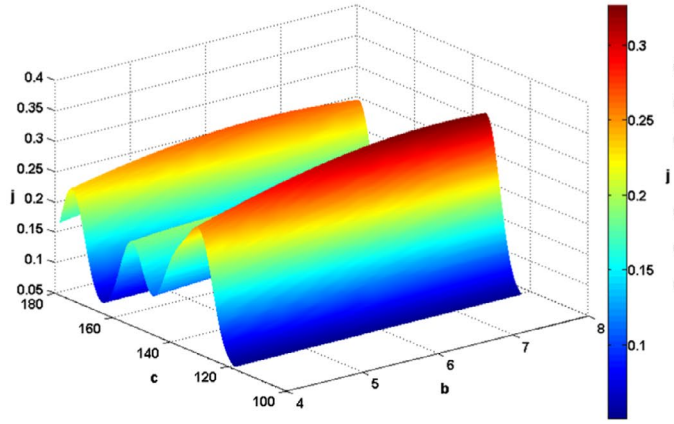

(C) *j vs c*, *b*

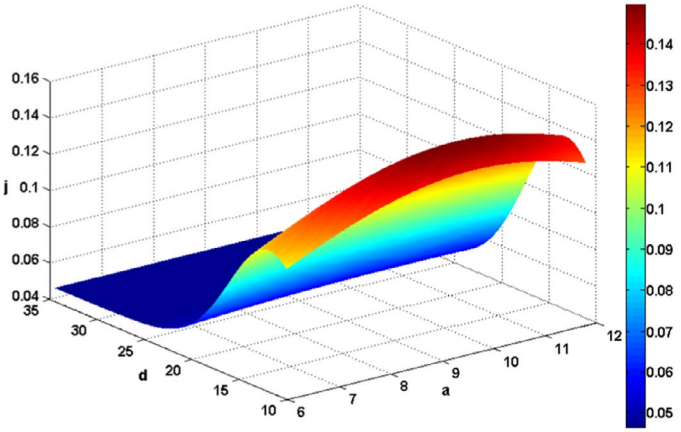

(D) *j vs d*, *a*

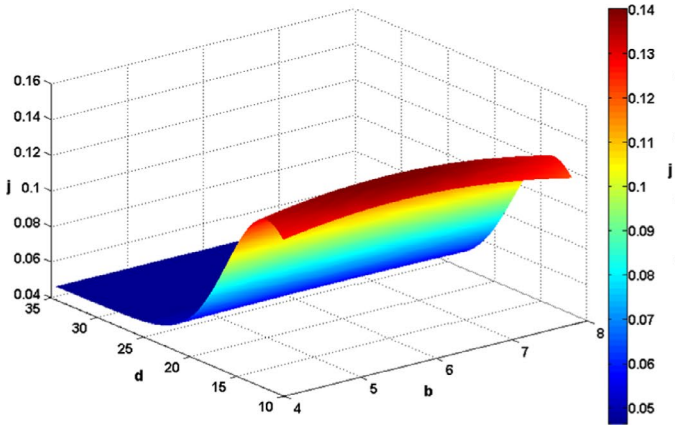

(E) *j vs d*, *b*

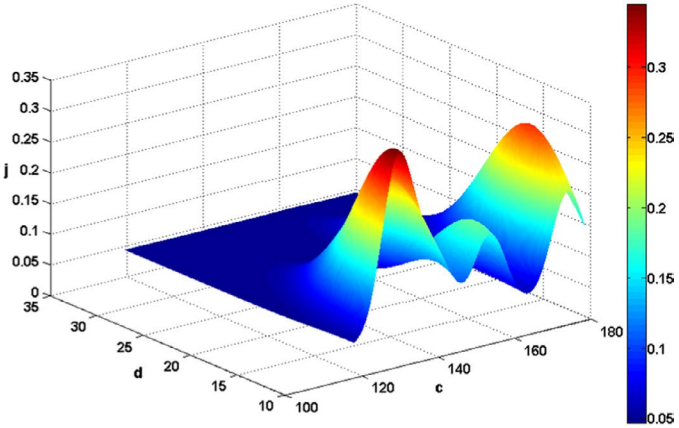

(F) *j vs d*, *c*

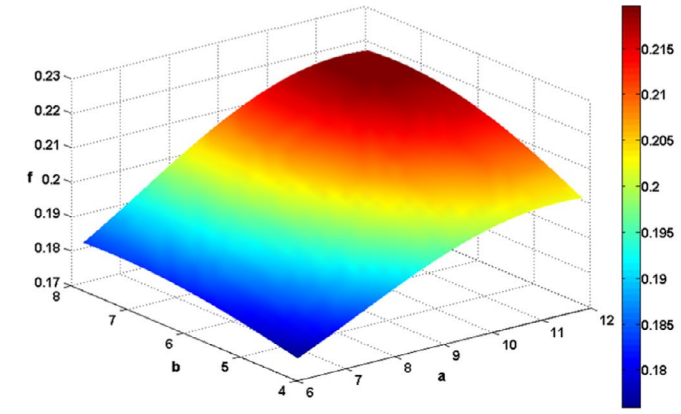

(G) f vs b, a

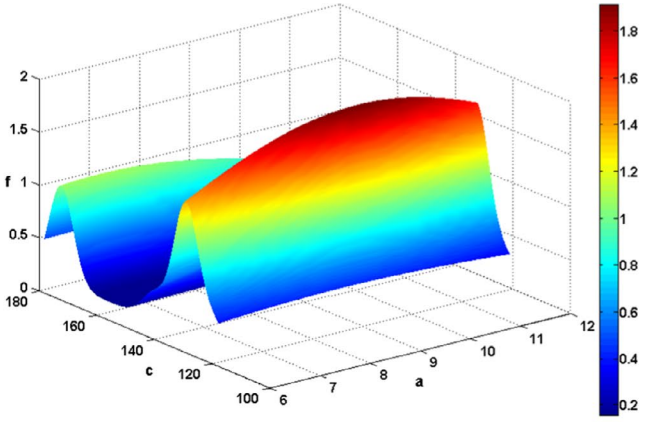

(H) f vs c, a

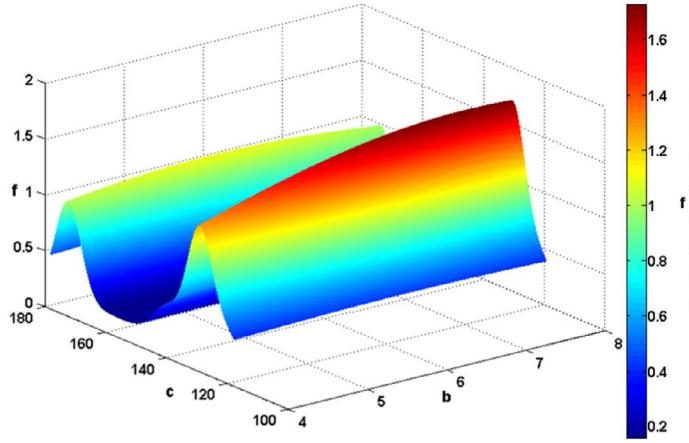

(I) f vs c, b

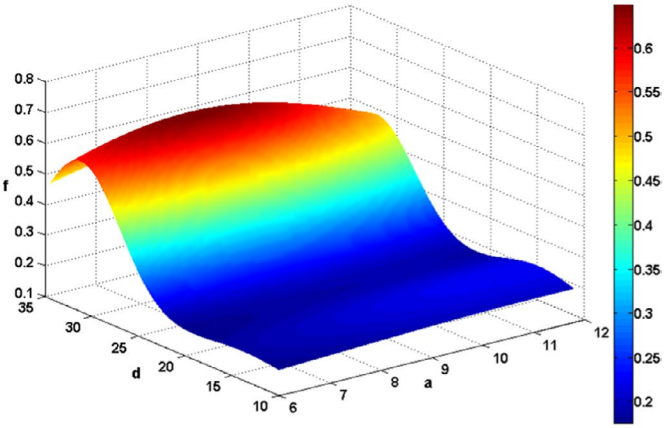

(J) f vs d, a

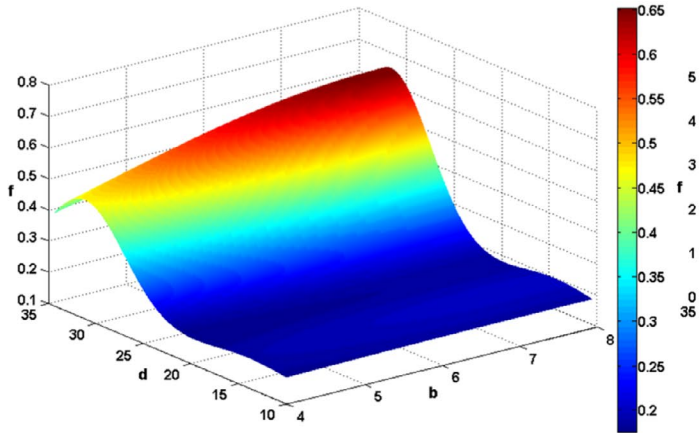

(K) f vs d, b

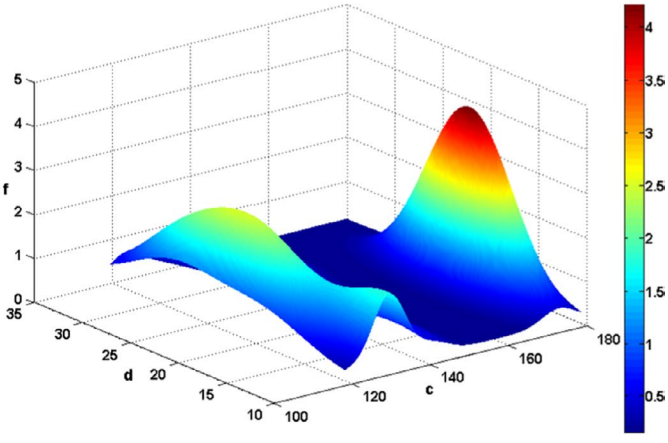

(L) f vs d, c